JOURNAL OF AIRCRAFT
Vol. 29, No. 5, Sept.–Oct. 1992

Dynamic Analysis of Rotor Blades with Root Retention Design Variations

R. G. Loewy,* A. Rosen,† M. B. Mathew,‡ and M. Zotto§
Rensselaer Polytechnic Institute, Troy, New York 12180

Kinematic and elastic couplings are often provided in rotor blade root retention systems to improve aeroelastic or flight stability. This paper uses the generalized coordinates approach and Lagrange Multiplier variational method to arrive at a unified formulation in which it is unnecessary to repeat the structural part of the analysis when root boundary conditions change. Such a method has advantages for evaluating design variations of blade retention systems. Two idealized rotor hub-hinge system models, with many features typical of advanced blade retention designs, are examined here. The in vacuo, free vibration characteristics of rotor blades with mass-elastic properties outboard of the attachment point typical of present-generation rotorcraft are calculated, as influenced by these retention systems. Trends with variations of root retention system parameters are presented for natural frequencies, damping ratios, and the amount of blade pitch induced by root flapping or lagging motions. A well-known static instability, which could be insidious in advanced rotor retention system design, is also reviewed.

Nomenclature (See Fig. 1)

C_ξ = damper viscous rate
EI_{yyf} = flexstrap bending rigidity in the flap direction
EI_{zzf} = flexstrap bending rigidity in the lag direction
e_j = hinge offset from center of rotation, for $j = \xi, \beta$
e_θ = pitch link in-plane offset from blade radial axis
GJ_f = flexstrap torsional rigidity
h = snubber spring vertical offset from plane of rotation
I_{yy} = rotor blade mass moment of inertia/length about an axis in chord plane, normal to radial axis and through section CG
I_{zz} = rotor blade mass moment of inertia/length about a vertical axis through section CG
k_c = control spring stiffness (acting at the pitch link)
k_j = angular spring rate, for $j = \xi, \beta$
k_j = linear spring restraint at blade root, for $j = y, z$
k_{sj} = snubber spring rate, for $j = \xi, \beta$
k_θ = blade root torsional spring rate
R = rotor radius
v = blade motion, in plane of rotation
w = blade motion, out of plane rotation
α_2 = pitch-lag coupling
δ_3 = pitch-flap coupling
ε_ξ = damper offset from blade radial axis
ν = rotor blade mass/length
ϕ = blade torsion angle
Ω = rotor speed
ω = blade coupled, rotating natural frequency
ω_j = blade cantilever, non-rotating natural frequency

Subscripts
b = blade
s = flexstrap
y = lead-lag direction
z = vertical direction
β = flap
ξ = lag

Introduction

ROTOR blade retention systems must carry the large centrifugal forces and large in-plane and out-of-plane forces and bending and torsional moments which put the helicopter in equilibrium, and also provide the blade pitch angle variations that achieve aerodynamically-based control. In the vast majority of rotor designs, provision for these control motions are made at the blade root as collective and cyclic blade pitch. Flapping and lagging hinges are also usually placed at or near the points of blade attachment to the hub, primarily to reduce the magnitude of the blade bending moments near the blade roots, where they would otherwise be greatest. Various kinds of so-called "kinematic couplings" are associated with blade motion about these hinges, when they are used, or with the motions allowed by so-called flexstraps, more recently used to replace hinges. Blade flap-pitch coupling δ_3 is often introduced, as is α_2, pitch-lag coupling.[1] The former is useful for augmenting longitudinal stability in forward flight, the latter in stabilizing aeroelastic instabilities involving the lowest lag mode.

Rotor hub mechanism designers attempt to eliminate the need for lubrication and reduce the wear and maintenance associated with conventional hinge bearings through the use of either flexstraps or elastomeric bearings. This can also reduce initial cost and hub and hinge cross-sectional areas, with attendant drag benefits in cruise flight. Flexstrap rotors and those with elastomeric bearings, of course, introduce new characteristics, as compared to conventional articulated rotors with mechanical bearings. All degrees of freedom now have, with these newer designs, substantially higher spring rates for angular motions, such are nominally zero for mechanical hinges. They may also have significantly lower elastic restraints for translational motions perpendicular to the blades' undeflected centerline. Furthermore, elastomeric bearings all introduce some damping for angular motions, although such will generally be small for flapping motions, compared to aerodynamic damping. The relatively small amount of damping avail-

Presented as Paper 90-1159 at the AIAA/ASME/ASCE/AHS/ASL 31st Structures, Structural Dynamics and Materials Conference, April 2–4, 1990; Long Beach, CA, received Dec. 17, 1990; revision received Oct. 9, 1991; accepted for publication Oct. 20, 1991.

*Institute Professor. Fellow AIAA.
†Senior Post Doctoral Fellow on Sabbatical leave; currently at Technion, Israel Institute of Technology, Haifa, Israel. Member AIAA.
‡Postdoctoral Fellow; currently Dynamics Engineer, Boeing Helicopter Co.
§Graduate Student, ARO Distinguished Fellow.

able through elastomeric bearings can be important for lag motions, however, since aerodynamic lag damping is low. Perhaps most important, with the constraint type of couplings being used in advanced rotor blade retention designs, the existence of elastic restraining forces provide additional load paths, and it is not as easy to predict what motions will result as it was when the couplings among the angular motions were purely kinematic.

Since advanced rotor designs are incorporating retention system components whose purposes go beyond structural considerations and providing basic flight control motions, the effect of variations in such design parameters are of major interest. In addition, the magnitude of the comprehensive programs used to predict the aeroelastic stability of coupled rotor-airframe systems, for example, or blade loads and response at high forward speeds or in maneuvers—of which the structural dynamic analysis is just one part—makes computational efficiency in analyses involving root retention system variations quite desirable. Modal methods provide such efficiency. An early blade analysis program making use of generalized coordinates to examine the effects of root retentions on the dynamics of a hingeless rotor is given in Ref. 2, which also incorporates some of the nonlinear equations of Ref. 3. The generalized coordinates approach was extended in Refs. 4 through 7 to deal with geometrically nonlinear cases by use of the Principal Curvature Transformation. A more recent extension of this approach[8] makes use of the classical Lagrange Multiplier variational method[9] to arrive at a unified structural dynamic formulation, which makes it unnecessary to repeat the structural part of the analysis when root boundary conditions change, as they do with design variations of blade retention systems.

Figure 1 shows an offset blade attachment point, including linear and angular springs at the flap and lag hinges, virtual δ_3 with control system spring, "equivalent α_2" with offset lag and flap "snubber" springs, and a lag damper. In this paper, three idealized rotor hub-hinge system models with many features typical of advanced rotor blade retention system designs (10) are examined (see Table 1). Cases I and II are fully articulated with coincident flap and lag hinges. The latter is typical of current practice, with 5% offset. The former has hinge offsets and elastic restraints about the hinges which simulate case III. Case III incorporates a beam-torsion member under axial load to represent a flexstrap extending to the blade attachment point at 26.8% R. In this linearized model, pitch and snubber arms are assumed infinitely rigid although in many advanced hub configurations, both pitch and snubber arm functions are incorporated in a "cuff" which is, in fact, flexible. The effect of cuff flexibility on aeroelastic stability has been considered in Refs. 10 and 11; Fig. 2 is repeated here from Ref. 11 for the purpose of comparison. In the present article, pitch and snubber arm flexibility are represented in gross terms by springs at their extremities (Fig. 1).

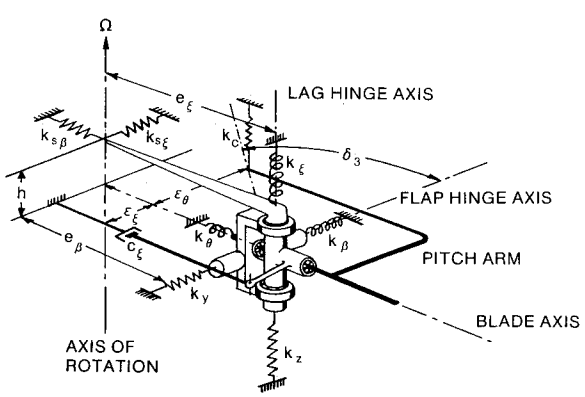

Fig. 1 Schematic of rotor root retention system mathematical model.

Table 1 Blade retention system properties

	Case I (Spring simulated flexstrap)	Case II (Articulated)	Case III (Flexstrap)
e_j, M	1.6383	0.3048	1.6383
ε_ξ, M	0.1270	0.1270	0.1270
e_θ, M	0.1715	0.1715	0.1715
h, M	0.0508	0.0508	0.0508
k_β, N-M/rad	0.3160×10^6	0	NA
k_ξ, N-M/rad	0.5020×10^6	0	NA
k_z, N/M	0.4730×10^6	∞	NA
k_y, N/M	0.67900×10^6	∞	NA
k_c, N/M	0.1749×10^7	0.1749×10^7	0.1749×10^7
k_θ, N/M/rad	0.3804×10^5	0.3804×10^5	NA
$k_{s\beta}$, N/M	0.1833×10^8	0	0.1833×10^8
$k_{s\xi}$, N/M	0.1751×10^6	0.1751×10^6	0.1751×10^6
C_ξ, M	0.1500×10^6	0.1500×10^6	0.1500×10^6
EI_{zz_f}, N-M^2	NA	NA	0.1850×10^6
EI_{yy_f}, N-M^2	NA	NA	0.6200×10^5
GJ_f, N-M^2	NA	NA	0.6232×10^5

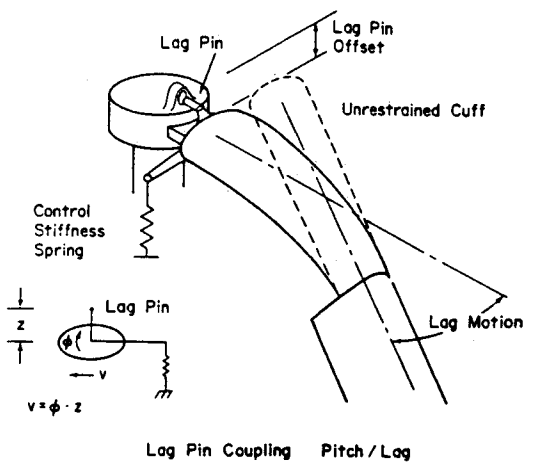

Fig. 2 Bearingless rotor blade with lag shear pin (from Ref. 11).

Review of Computational Method

Two kinds of equations are used to solve for the in vacuo modes of rotor blades with various root retention arrangements. First, the equations of motion for free vibration, written in terms of N generalized coordinates, q_i

$$[A]\{\ddot{q}\} + [B]\{\dot{q}\} + [C]\{q\} = 0 \tag{1}$$

where $\{q\}$ is a vector of Nth order.$[A]$, $[B]$, and $[C]$ are $N \times N$ square matrices.

Second, a system of equations representing constraints introduced by the root retention system. This second set can be dealt with in two distinct approaches. The first approach, using Lagrange Multipliers, expresses constraint equations (at the root or elsewhere) as

$$[R_1]\{\dot{q}\} + [R_2]\{q\} = \{r\} \tag{2}$$

The order of the matrices $[R_1]$ and $[R_2]$ is $N_\lambda \times N$, and that of the vector is N_λ, where N_λ is the number of constraint equations.

As explained more fully in Ref. 8, the technique of Lagrange Multipliers then allows these equations to be combined in state vector form; i.e., where $\{X\}^t \triangleq \langle\{\dot{q}\}^t, (q)^t, (\lambda)^t\rangle$ as follows:

$$\begin{bmatrix} [A1] & 0 & [R_4] \\ 0 & [I] & 0 \\ 0 & 0 & 0 \end{bmatrix} \{\dot{X}\} + \begin{bmatrix} [B] & [C] & [R_3] \\ [-I] & 0 & 0 \\ [R_2] & [R_1] & 0 \end{bmatrix} \{X\} = \begin{Bmatrix} 0 \\ 0 \\ \{r\} \end{Bmatrix} \tag{3}$$

where λ are the unknown Lagrange Multipliers[9] and $[I]$ is the identity matrix. This formulation is sufficiently general to account for geometrically nonlinear situations. For linear cases, i.e., where $[R_1]$ and $[R_2]$ are not functions of $\{q\}$ or $\{\dot{q}\}$, $[R_3] = [R_1]^t$; $[R_4] = [R_2]^t$; and $[A1] = [A]$.

In the second approach, Eq. (1) is written with the constraints represented by a "pseudo forcing function"

$$[A\{\ddot{q}\} + [B]\{\dot{q}\} + [C]\{q\} = \{f_r\} \tag{4}$$

where the generalized forces $\{f_r\}$ are thought of as imposed on the flexible blade by the root retention system. Since these root-imposed generalized forces are expressed in terms of the root deflections and elastic constraints, they can then be taken to the left-hand side of Eq. (4); i.e., $\{f_r\}$ is expressed as

$$\{f_r\} = [A_r]\{\ddot{q}\} + [B_r]\{\dot{q}\} + [C_r]\{q\} + \{d\} \tag{5}$$

and Eq. (4) becomes

$$[\tilde{A}\{\ddot{q}\} + [\tilde{B}]\{\dot{q}\} + [\tilde{C}]\{q\} = \{d\} \tag{6}$$

in which

$$[\tilde{A}] = [A] - [A_r], \quad [\tilde{B}] = [B] - [B_r]$$
$$[\tilde{C}] = [C] - [C_r] \tag{7}$$

The elements of the $N \times N$ square matrices $[A_r]$, $[B_r]$ and $[C_r]$ can be evaluated using, for example, virtual work principles.

Choice of Generalized Coordinates

To minimize recalculation of blade structural contributions as root boundary conditions change, the modes to be used as the shape functions associated with generalized coordinates are chosen as cantilever modes

$$\begin{aligned} &FV_{(j)}(x = 0) = FV'_{(j)}(x = 0) = 0 && \text{for } j \geq 3 \\ &FW_{(k)}(x = 0) = FW'_{(k)}(x = 0) = 0 && \text{for } k \geq 3 \\ &F\phi_{(l)}(x = 0) = 0 && \text{for } l \geq 2 \end{aligned} \tag{8}$$

here V implies in-plane motion, W out-of-plane motion, and ϕ torsional motion of the blade elements.

Following procedures described in Refs. 4 through 8, the specific modal functions used as generalized coordinates are the uncoupled nonrotating, in vacuo modes of the subject blade neglecting any twist, droop, sweep, or precone and assuming that the blade section centers of gravity are on the elastic axis. Note that the modal indices j, k, and l in Eq. (8) are initiated at 3, 3, and 2, respectively, to allow for rigid body translational and rotational DOF at the blade attachment points, as follows:

$$\begin{aligned} FV_{(1)} &= FW_{(1)} = F\phi_{(1)} = 1 \\ FV_{(2)} &= FW_{(2)} = x \end{aligned} \tag{9}$$

Following nomenclature and conventions as shown in Fig. 3, displacements are defined in terms of the generalized coordinates, as follows:

$$\begin{aligned} u &= u_0 + \sum_{n=1}^{N_u} q_{u(n)} FU_{(n)} \\ v &= \sum_{j=1}^{N_v} q_{v(j)} FV_{(j)} \\ w &= \sum_{k=1}^{N_w} q_{w(k)} FW_{(k)} \\ \phi &= \sum_{l=1}^{N_\phi} q_{\phi(l)} F\phi_{(l)} \end{aligned} \tag{10}$$

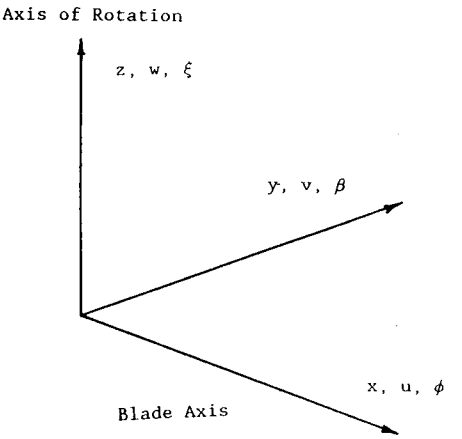

Fig. 3 Coordinate axis definition and sign convention.

Here, $q_{v(j)}$, $q_{w(k)}$, and $q_{\phi(l)}$ are the generalized coordinates, functions of time. Displacements in the x (i.e., radial) direction $q_{u(n)}$ are known functions of $q_{v(j)}$ and $q_{w(k)}$ since the blade is assumed radially inextensible. On this basis, the vector of unknown generalized coordinates becomes

$$\begin{aligned} \{q\}^t = \langle & q_{v(1)}, \ldots, q_{v(j)}, \ldots, q_{v(N_v)} \\ & q_{w(1)}, \ldots, q_{w(k)}, \ldots, q_{w(N_w)} \\ & q_{\phi(1)}, \ldots, q_{\phi(l)}, \ldots, q_{\phi(N_\phi)} \rangle \end{aligned} \tag{11}$$

where $N = N_v + N_w + N_\phi$.

For details of the derivation of the matrices $[A]$, $[B]$, and $[C]$ in Eq. (1) accounting for rotational effects; blade twist, droop, sweep, precone and/or the associated predeformations; section mass chordwise offset from the elastic axis; and geometric nonlinearities, see Refs. 4 through 6.

Once the analysis is in the form shown in Eq. (3) or Eq. (6), standard root-finding techniques can be used to evaluate the complex eigenvalues and eigenvectors and Eqs. (10) used to determine the associated mode shapes.

Cases Analyzed

Rotors intended to be roughly light attack/scout helicopter-size were postulated, with uniform properties spanwise, giving the natural, uncoupled, in vacuo nonrotating, cantilever-free frequencies listed in Table 2.

Case I is articulated, with hinge spring rates chosen to simulate the specific flexstrap rotor of case III at $\Omega = 286$ rpm. Case II is a more typical, fully articulated rotor with 5% flap and lag hinge offsets. These three configurations are considered "base cases," and certain of their characteristics varied to establish the trends presented in the following section.

The lowest four lag modes, four flap modes and two torsion modes plus the five rigid body DOF represented in Eq. (9) were included in the analyses. Figure 4 shows the degree of convergence achieved with these 15 DOF and the subject analysis method, using the case I properties.

Numerical Results

Articulated Rotor with δ_3

A special articulated version of the case I rotor with zero flap and lag hinge offsets was analyzed, in which e_β, e_ξ, k_β, k_ξ, k_θ, $k_{s\beta}$, and C_ξ, were all set equal to zero and k_y and k_z were made infinitely stiff. Solutions of Eq. (3) for $\Omega = 286$ rpm are shown in Fig. 5 as a function of δ_3 and for several values of control spring stiffness k_c. Since e_θ is held constant as δ_3 varies, a value of δ_3 equal to 90 deg can only be ap-

Table 2 Blade properties and cantilever nonrotating frequencies

	Cases I & III	Case II
R, M	6.096	6.096
ν, Kg/M	0.1434×10^{2}	0.1136×10^{2}
I_{zz}, Kg-M	0.1768	0.1401
I_{yy}, Kg-M	0.8421×10^{-2}	0.6671×10^{-2}
Modal type and number	(rad/s)	(rad/s)
ω_ξ 1	33.1	37.1
2	207.2	232.7
3	580.1	651.9
4	1136.7	1277.1
5	1879.0	2111.1
ω_β 1	7.2	8.1
2	45.2	50.7
3	126.5	142.1
4	247.8	278.5
5	409.7	460.3
ω_ϕ 1	160.4	180.2
2	481.1	540.6
3	801.9	900.9
4	1122.7	1261.3
5	1443.4	1621.7

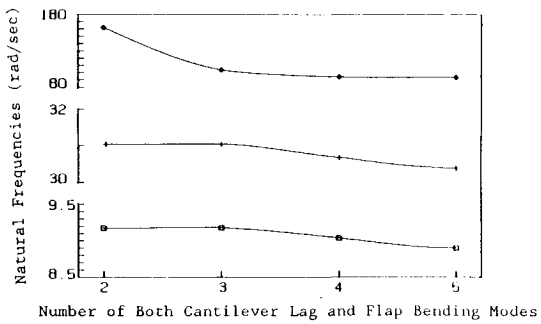

Fig. 4 Convergence of first three modes as a function of the number of cantilever bending modes used as generalized coordinates (case I).

proached. At that point, the flap and pitch frequencies approach each other and rotor speed. The first torsion mode is sensitive to control spring variations, as expected, and second flap is strongly coupled to first torsion at the highest δ_3 values. In fact, the second mode becomes pitch-torsion and the third mode largely second flap bending at that point.

As some indication of the influence of nonlinear effects, this same case was studied at $\delta_3 = -30$ deg but with coning and pitch "predeformations" set arbitrarily at 5.73 deg and 8.3 deg, respectively. The first lag, flap, and torsion mode shapes which result are shown in Figs. 6a, 6b, and 6c, respectively. Their principal deflection component was normalized to one meter or one radian, as appropriate. Coriolis forces and principal axes of cross-sections being out of the plane of rotation now couple lag, flap and pitch motions, formerly only coupled by δ_3. Further, Coriolis forces introduce motion components 90 deg out of phase, shown in these figures as imaginary and real components. Figure 6a shows that for a tip lag displacement of, say, 0.1 m, there exist tip pitch angle changes of about 0.25 deg, as well. Figure 6b indicates that about 0.8 deg pitch change occurs at the blade tip with 0.1-m flap deflection; this compares with only 0.5 deg that would be expected with a rigid control link. Apparently dynamic amplification is occurring, although tip pitch (ϕ) and tip flapping (w) are close to being in phase.

Articulated Rotor with δ_3 and α_2

A series of calculations were run for the case II, typical articulated configuration, to investigate the degree to which "kinematic couplings" would be achieved with flexible com-

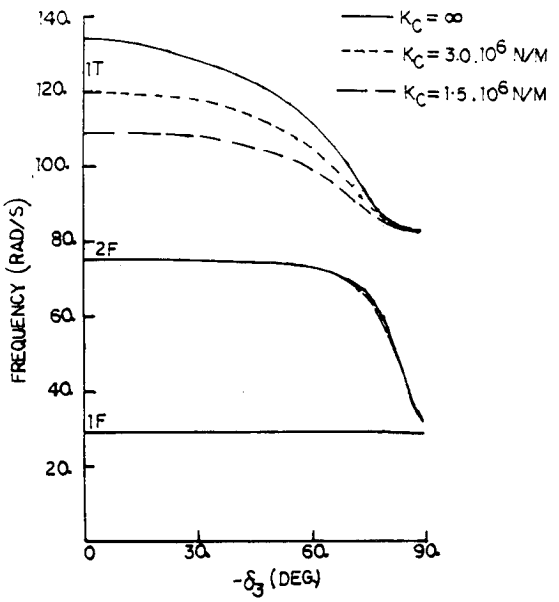

Fig. 5 Influence of virtual δ_3 on the frequencies of the first three flap/torsion modes of vibration (case I—specialized; Ω = 286 rpm).

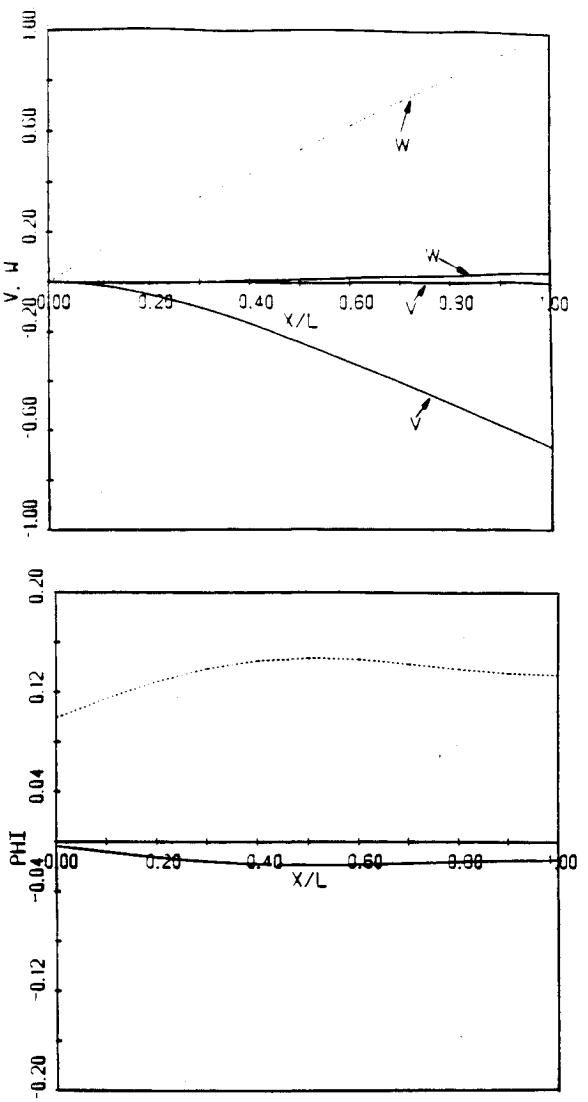

Fig. 6a First flap mode shape: ω = 30.46 rad/s. Dashed lines are real components; solid lines are imaginary components (case I—specialized; Ω = 286 rpm; $\delta_3 = -30$ deg; rigid flap predeformation = 5.73 deg; and pitch predeformation = 3.3 deg).

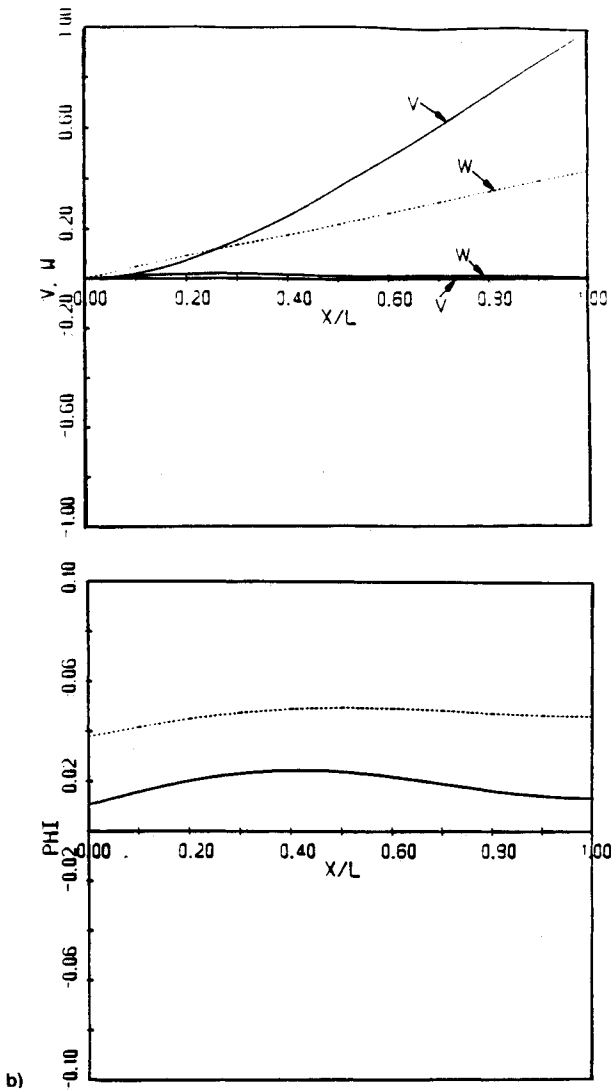

b)

Fig. 6b First lag mode shape: ω = 23.77 rad/s. Dashed lines are real components; solid lines are imaginary components (case I—specialized; Ω = 286 rpm; δ_3 = −30 deg; rigid flap predeformation = 5.73 deg; and pitch predeformation = 3.3 deg).

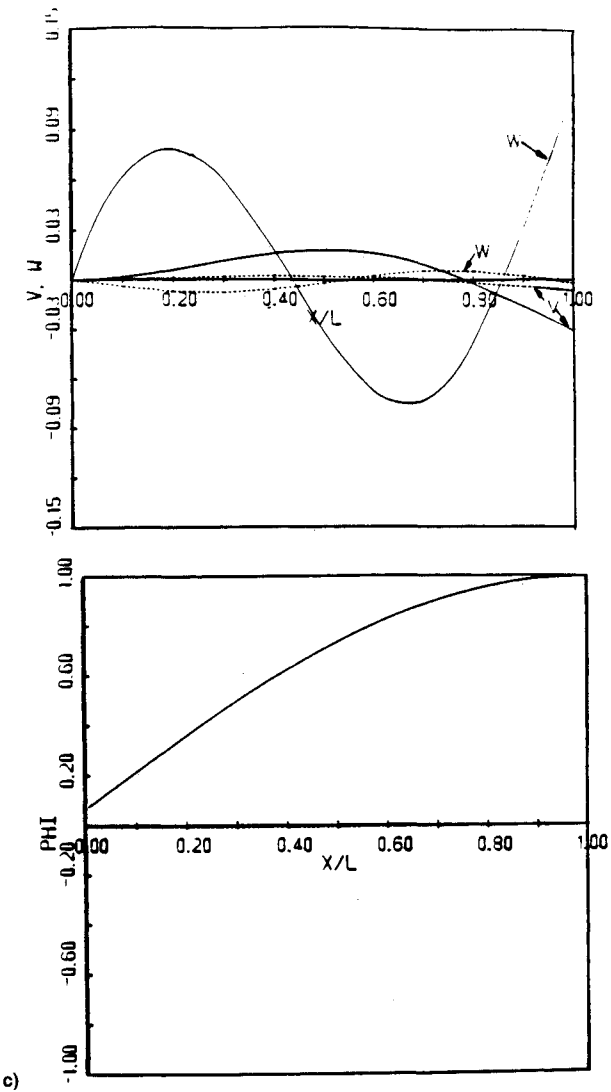

c)

Fig. 6c First torsion mode shape: ω = 126.8 rad/s. Dashed lines are real components; solid lines are imaginary components (case I—specialized; Ω = 286 rpm; δ_3 = −30 deg; rigid flap predeformation = 5.73 deg; and pitch predeformation = 3.3 deg).

ponents. The method used here and in the following cases solved the equations of motion in Eq. (6) form. Rather than present the results as pitch-torsion angles in normalized modes, however, ratios of those values to what would have been achieved if the pertinent system elements were rigid (the "kinematic" values) are calculated and shown in the following figures. That is, with a rigid control system and blade (k_c = ∞; GJ_b = ∞) and δ_3, one would expect the pitch angle at the blade tip sections in response to flapping to be

$$|\phi_{\text{tip}}|_{\text{Kinematic}_{\delta_3}} = (\tan \delta_3)|\beta| = (\tan \delta_3) \left| \frac{w_{\text{tip}}}{R - e_\beta} \right| \quad (12a)$$

Similarly, with a rigid snubber spring and blade ($k_{s\xi}$ = ∞; GJ_b = ∞) and effective α_2, one would expect

$$|\phi_{\text{tip}}|_{\text{Kinematic}_{\alpha_2}} = \frac{e_\xi}{h}|\xi| = \frac{e_\xi}{h} \left| \frac{v_{\text{tip}}}{R - e_\xi} \right| \quad (12b)$$

Figure 7a shows, for a configuration like the case II rotor blade retention system combination but with snubber spring offset, h = 0.2032 and root torsional restraint k_θ = 190, that the higher the value of intended δ_3, the smaller will be the percentage of that value actually achieved in the first flap mode. It also shows, as one might expect, that the stiffer the control spring, k_c, the closer will be the value achieved to that intended, for any particular value of δ_3. The abscissa was chosen for this and subsequent charts as a ratio of elastic restraint terms which produce blade pitch moments in response to blade flapping motion divided by the elastic restraint terms which resist blade pitching motions. Note that a control spring stiffness, k_c = 1.7 × 10^4, seems quite "soft" relative to the objective of producing δ_3 coupling. Figure 7b is identical to Fig. 7a except that the root torsional restraint k_θ has been increased to the base value in case II. Comparing these two figures shows that the achievable δ_3 drops as the stiffness of springs restraining pitch motions increases.

Figure 8 is similar to Fig. 7, but in this case the α_2 pitch response to lag motion in the fundamental lead lag mode is shown for a number of lag snubber spring offsets h and control spring stiffnesses. Note that increasing snubber spring offset is helpful in approaching kinematic coupling ratios. Increasing control spring stiffness at constant h is, on the other hand and as might be expected, counterproductive for α_2 effect, since k_c is one of the pitch restraint springs that must be overcome (see denominator of the abscissa) in producing blade pitching motion.

One more evaluation of articulated system characteristics was made, to assess the influence of lag angular spring rates k_ξ of the sort encountered with elastomeric lag bearings. Here the case II configuration but with ½ nominal root torsional

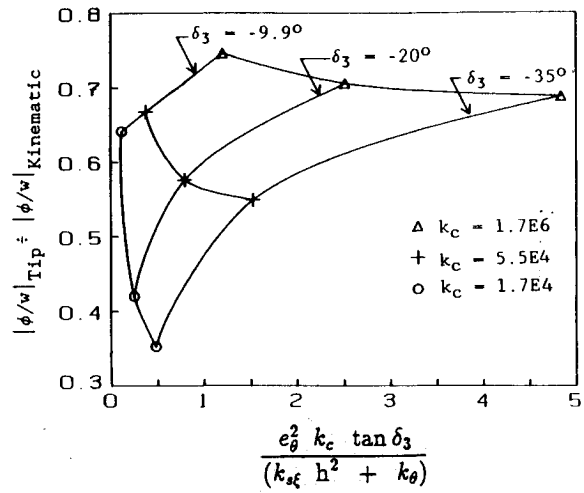

a)

Fig. 7a Effective δ_3 as fraction of kinematic values vs control spring parameter (case II, except k_θ = 190; and h = 0.2032).

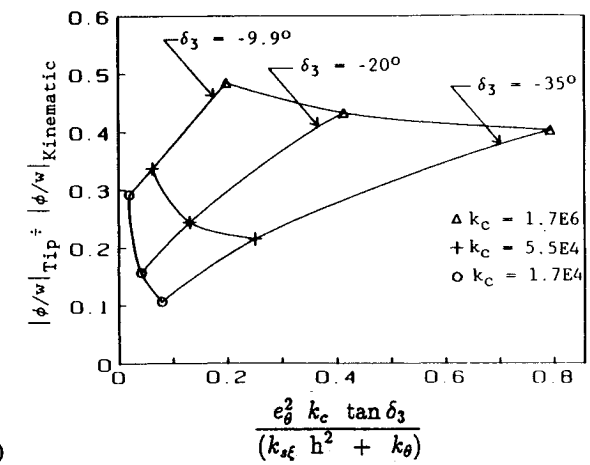

b)

Fig. 7b Effective δ_3 as fraction of kinematic values vs control spring parameter (case II, except h = 0.2032).

restraint k_θ was examined for the effect of k_ξ on the ratio of damping in the first predominantly lag mode to critical. Because the frequency of this mode is directly affected by k_ξ changes and because critical damping is linearly proportional to natural frequency, both damping ratios and natural frequencies were normalized by the values of these same quantities calculated for the corresponding rigid blade, single DOF in lag cases. The results are presented in Fig. 9, showing that both critical damping ratios and natural frequencies in these lowest lag modes decrease relative to the rigid blade, single degree-of-freedom values as k_ξ increases. One set of curves in Fig. 9 includes the effect of the lag snubber spring, $k_{s\xi}$ on rigid blade, single degree-of-freedom characteristics (and on abscissa values), and one set does not. As a matter of reference, the expressions used for the rigid blade, single degree-of-freedom cases are

$$\omega_\xi = \Omega\sqrt{\frac{3e_\xi}{2(R-e_\xi)} + \frac{3(k_\xi + k_{s\xi}e_\xi^2)}{\nu(R-e_\xi)^3\Omega^2}}$$

$$\left(\frac{C}{C_{\text{crit}}}\right)_\xi = \frac{C_\xi e_\xi^2}{2\Omega\sqrt{\frac{\nu(R-e_\xi)^3}{3}\left(\frac{e_\xi\nu(R-e_\xi)^2}{2} + \frac{k_\xi + k_{s\xi}e_\xi^2}{\Omega^2}\right)}} \tag{13}$$

For the case II parameters, the term $k_{s\xi}e_\beta^2$, which appears in both expressions, has a relatively small effect except for values of k_ξ near zero. Not shown in Fig. 9 is the fact that increasing blade mass per unit length to the case I and III values, keeping all other characteristics the same, changed the results given there by less than 5%.

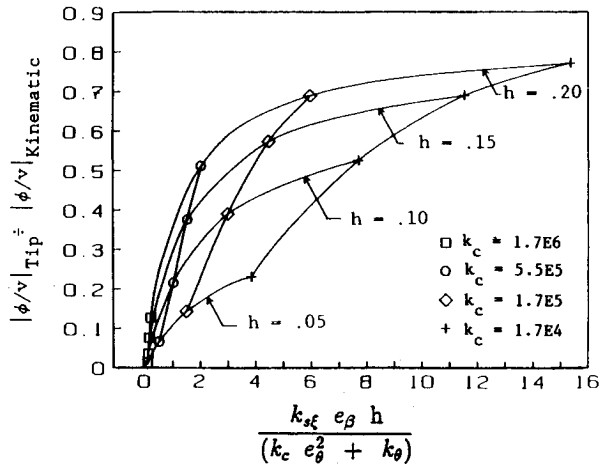

Fig. 8 Effective α_2 as fraction of kinematic value vs lag snubber spring parameter (case II, except k_θ = 190; and δ_3 = −35 deg).

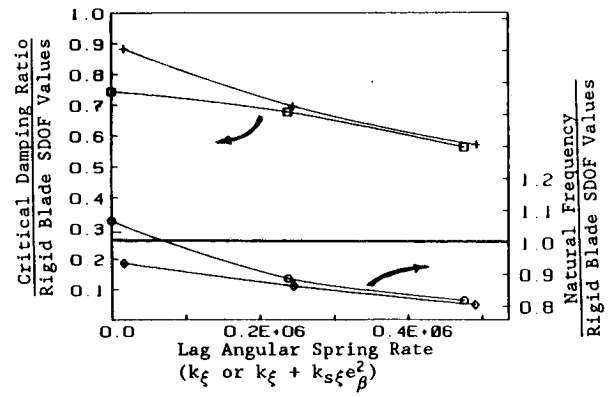

Fig. 9 First lag mode characteristics relative to those of a single degree-of-freedom rigid blade vs lag angular spring stiffness (case II, except k_θ = 0.1902 × 10^5).

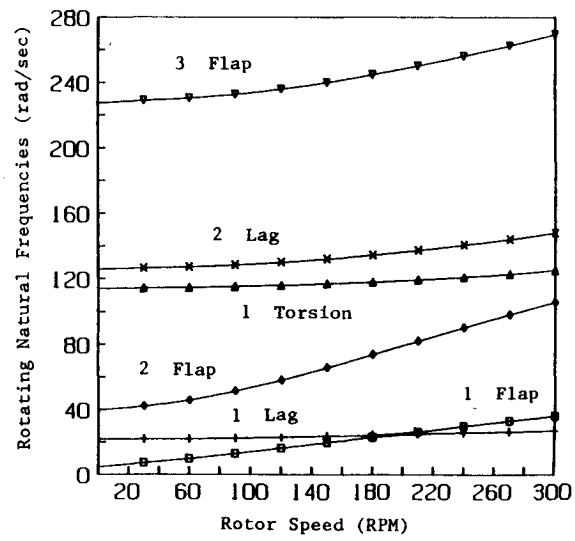

Fig. 10 Variation of the first six rotating natural frequencies with revolutions per minute (case III).

Flexstrap Rotor

Case III represents a flexstrap rotor with values representative of recent designs. The Campbell diagram for this configuration is shown in Fig. 10. A slight reduction of first lag mode natural frequencies with increasing rotor speed beyong 300 rpm prompted an investigation using the "equivalent" articulated arrangement of case I, with the flexstrap retention effects represented by root end stiffness influence

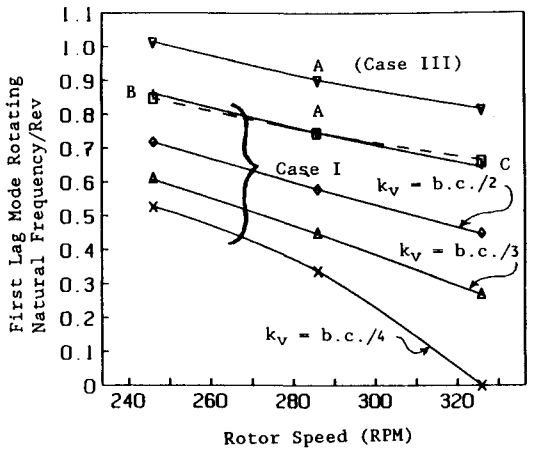

Fig. 11 Effect of linear lag spring stiffness on centrifugal divergence stability (cases I and III).

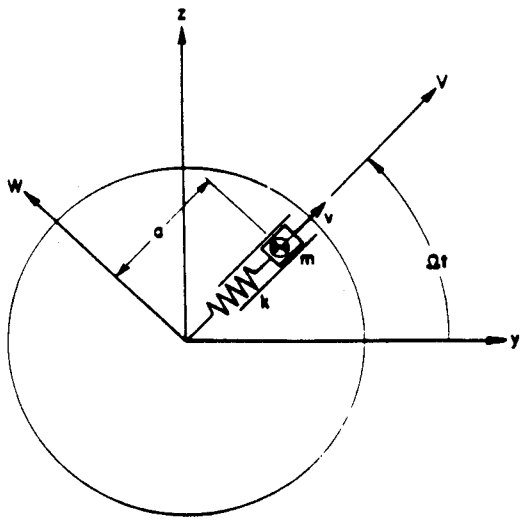

Fig. 12 Rotating disk containing a spring-restrained mass in a radial slot.

coefficients, i.e., by the equation

$$\left|\begin{array}{c}\text{Force}\\ \text{Moment}\end{array}\right|_{\text{lag}} = \left|\begin{array}{cc|cc||c}a_{11} & a_{12} & a_{13} & a_{14} & v\\ a_{21} & a_{22} & a_{23} & a_{24} & \xi\\ \hline a_{31} & a_{32} & a_{33} & a_{34} & w\\ a_{41} & a_{42} & a_{43} & a_{44} & \beta\end{array}\right| \quad (14)$$

$$\left|\begin{array}{c}\text{Force}\\ \text{Moment}\end{array}\right|_{\text{flap}}$$

The coefficients a_{ij} were calculated using a static, transfer matrix analysis accounting for axial load and twist, linearized for small deflections. Torsion was handled independently. Thus, case I and case III would be identical, if $k_\beta = a_{44}$; $k_\xi = a_{22}$; $k_z = a_{33}$; $k_y = a_{11}$, except that the terms a_{ij} (where $i \neq j$) would be ignored in case I. The off-diagonal partitioned matrices are identically zero if the flexstrap is untwisted, as in case III. The points A in Fig. 11 compare rotating natural frequencies for the first primarily lag mode calculated using the case III representation [i.e., Eq. (14)] with that calculated using the corresponding case I (i.e., dropping a_{ij}, where $i \neq j$, terms). These elastic cross-coupling terms are seen to raise this natural frequency appreciably. The dashed curve through points, B, A, and C reflect flexstrap stiffening under the influence of centrifugal force as calculated in the full case III results. The corresponding solid line is for case I, in which equivalent spring stiffnesses have not been changed with revolutions per minute. The remaining case I curves in Fig. 11 have been calculated with fixed equivalent spring rates, but at various fractions of the base case (b.c.) linear lag spring,

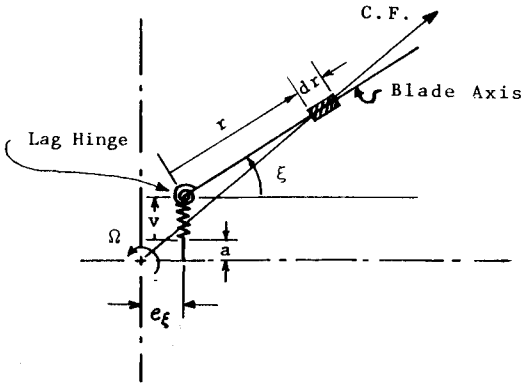

Fig. 13 Two-degree-of-freedom rigid blade, in-plane model.

k_v. The zero frequency at $\Omega = 326$ rpm for the case with k_v equal to $\frac{1}{4}$ the base value, indicates a static instability.

This type of instability is well known, often associated with rotating shafts. Figure 12 is repeated here from Ref. 13. The similarity to Fig. 13, a two-degree-of-freedom rigid blade on linear and angular lag springs, is clear. Divergence rotational speeds are

$$\Omega_{\text{div}} = \sqrt{k/m}$$

for the configuration in Fig. 11 and

$$\Omega_{\text{div}} = \sqrt{\frac{1}{2}\frac{k_y\left(e_\xi - \dfrac{k_\xi}{k_y\bar{r}}\right)}{m(e_\xi + \bar{r})}\left(1 \pm \sqrt{1 + \frac{4k_\xi(e_\xi + \bar{r})}{\bar{r}k_y\left(e_\xi - \dfrac{k_\xi}{k_y\bar{r}}\right)^2}}\right)} \quad (15)$$

for the configuration in Fig. 12. (The latter expression has a trivial root, $\Omega = 0$, where $k_\xi = 0$ and complex roots where $k_\xi \neq 0$, associated with the minus sign under the radical.) In the rotor case, $m \triangleq \nu(R - e_\xi)$ and $\bar{r} = (R - e_\xi)/2$.

The instability at $\Omega = 326$ rpm in Fig. 11 compares with a value of 390 rpm for the equivalent rigid blade case, i.e., using Eq. (15). The difference is a measure of the influence, primarily, of blade bending flexibility, and to a lesser extent, of the additional complications of lag snubber spring and δ_3 forcing the blade to pitch and flap together with this predominantly in-plane motion.

For reasonable flexstrap designs, this in-plane divergence would not seem likely to be encountered. Where elastomeric bearings are used in articulated designs, however, it is not so clear. It seems worthy of note, for example, that loads normal to the blade axis in the plane of rotation are primarily due to aerodynamic drag and Coriolis forces and, therefore, are small relative to lift and centrifugal forces. In providing sufficient strength to carry in-plane shear loads, say, parallel to the axis of an elastomeric flap bearing, it is important that the corresponding spring rate k_y be high enough to preclude this in-plane centrifugal divergence in the operating rotor speed range.

Conclusions

By combining generalized coordinate techniques, particularly those capable of dealing with geometric nonlinearities, with techniques for numerically accounting for constraints such as are encountered with advanced blade root retention systems, unified methods for structural dynamic design analyses can be formulated which have high computational efficiency. One such formulation using Lagrange Multipliers and/or pseudo forcing functions is presented here. Application to root retention configurations with wide variations in operating and design parameters shows that couplings such as δ_3 and α_2 and ratios of damping to critical values can differ substantially

from what would be predicted using simpler mathematical models. This study also suggests that in-plane spring rates in blade retention system designs should be checked to insure that centrifugal divergence instabilities will not be encountered in the rotor operating range. In-plane radial loads are so great that there is virtually no chance that such an instability will be incurred as a result of radial spring rates; for in-plane loads normal to the blade axis, it is not so obvious.

Acknowledgment

The work whose results are reported here was conducted under Army Research Office Rotorcraft Technology Center of Excellence Contract DAA LO3-88-C-004 as part of a larger study of rotor maneuver dynamics. The contract monitor was Gary Anderson.

References

[1]Bramwell A. R. S., *Helicopter Dynamics*, Wiley, New York, 1976.

[2]Sopher, R., and Cassarino, S. J., "Effects of Analytical Modeling Assumptions on the Predicted Stability of a Model Hingeless Rotor," *American Helicopter Society Journal*, Vol. 33, No. 4, 1988.

[3]Hodges, D. H., and Dowell, E. H., "Nonlinear Equations of Motion for the Elastic Bending and Torsion of Twisted Nonuniform Rotor Blades," NASA TN-D-7818, Dec. 1974.

[4]Rosen, A., Loewy, R. G., and Mathew, M. B., "Nonlinear Analysis of Pretwisted Rods Using Principal Curvature Transformation Part I: Theoretical Derivation," *AIAA Journal*, Vol. 25, No. 3, 1987, pp. 470–478.

[5]Rosen, A., Loewy, R. G., and Mathew, M. B., "Nonlinear Analysis of Pretwisted Rods Using Principal Curvature Transformation Part II: Numerical Results," *AIAA Journal*, Vol. 25, No. 4, 1987, pp. 598–604.

[6]Rosen, A., Loewy, R. G., and Mathew, M. B., "Nonlinear Dynamics of Slender Rods," *AIAA Journal*, Vol. 25, No. 4, 1987, pp. 611–619.

[7]Rosen, A., Loewy, R. G., and Mathew, M. B., "Application of the Principal Curvature Transformation to Nonlinear Rotor Blade Analysis," *Vertica*, Vol. 11, No. 1/2, 1987, pp. 263–296.

[8]Rosen, A., Loewy, R. G., and Mathew, M. B., "A Unified Treatment for Dealing with Auxiliary Conditions in Blade Dynamics," *AIAA Journal*, Vol. 29, No. 6, June 1991.

[9]Hsu, J. C., and Meyer, A. V., *Modern Control, Principles and Applications*, Chapter 13, "Calculus of Variations and Optimal Control." McGraw-Hill, New York, 1968, pp. 494–543.

[10]Bousman, W. G., Ormiston, R. A., and Mirick, P. H., "Design Considerations for Bearingless Rotor Hubs," *Proceedings of the 39th Annual American Helicopter Society Forum*, May 9–11, 1983.

[11]Dull, A. L., and Chopra, I., "Aeroelastic Stability of Bearingless Rotors in Forward Flight," *Proceedings of the 43rd Annual Forum of the American Helicopter Society*, St. Louis, MO, May 18–20, 1987.

[12]Wang, J. M., Chopra, I., Samak, D. K., Green, M., and Graham, R., "Theoretical and Experimental Investigation of the Aeroelastic Stability of an Advanced Bearingless Rotor in Hover and Forward Flight," *Proceedings of the AHS National Specialists' Meeting on Rotorcraft Dynamics*, Arlington, TX, Nov. 13–14. 1989.

[13]Loewy, R. G., and Piarulli, V. J., "Dynamics of Rotating Shafts," Shock and Vibration Information Center, U.S. Dept. of Defense, Naval Research Lab., Washington, DC, Library of Congress Catalog Card No. 70-606276, 1969.